Lasers in Manufacturing and Materials Processing (2021) 8:60–72
https://doi.org/10.1007/s40516-021-00137-3

Seam Formation in Laser Beam Micro-Welding with Spatial Power Modulation

Mirko Aden[1] · Paul Heinen[1] · Alexander Olowinsky[1]

Accepted: 27 January 2021 / Published online: 6 March 2021

Abstract

When laser sources of high brilliance are used for the micro-welding of metals, small seam dimensions are generated. If the spatial power is modulated by a superposition of the linear feed rate and a circular-oscillatory movement of high frequency, the width of the seam is controlled by the amplitude of the circular movement. In this study, the irradiation pattern of the seam was calculated and reveals that some spots of the seam area are not irradiated, while other have been irradiated several times. The seam shapes were visualized with micro cross-sections for different laser powers, linear feed rates and oscillatory amplitudes. Thermal simulations were made to discuss the different seam shapes. A consequence of the oscillatory movement is the appearance of different solidification fronts, which are visible in the micro cross-sections.

Keywords Laser beam micro-welding · Spatial power modulation · Seam geometry · Thermal simulation

Introduction

During the last few years laser beam sources with high brilliance and high beam quality have been developed at a fast pace. Such high beam qualities result in small focal diameters and high intensities, also for laser operation in cw-mode. Thanks to this, the radiation energy can be delivered precisely and on a small scale, enabling micro-welding of assemblies with dimensions in the sub-millimetre range. Examples can be found in all kind of technologies, reaching from welding of battery assemblies and electrical contacts via applications in telecommunication all the way to the use in components for satellites. For all applications, a high reproducibility and low energy input is necessary to avoid distortion or damage on connecting parts [1, 2].

✉ Mirko Aden
mirko.aden@ilt.fraunhofer.de

[1] Fraunhofer Institute for Laser Technology, Steinbachstraße 15, 52074 Aachen, Germany

In order to minimize the energy input to the assembly, but to create a sufficient weld depth, the laser welding process has to be run in the so-called deep-penetration regime. Deep-penetration welding with laser radiation has been investigated since the early 70s (e.g. [3]). In this process, laser-induced vaporization leads to a cavity in the parts, which is called a "keyhole". The depth of the keyhole determines the depth of the seam significantly. Furthermore, due to its high aspect ratio (depth/width), the keyhole acts as a beam trap. Since there are multiple reflections inside the cavity, the largest part of the laser beam is absorbed [4]. Thus, for deep-penetration welding the laser energy is converted effectively into heat, even for highly reflective materials such as copper [5, 6]. The onset of deep-penetration welding is a function of the beam intensity [5, 7]. For intensities below a critical value, welding occurs in the heat conduction regime, for higher intensities in the deep-penetration regime.

Although small beam diameters ensure intensities appropriate for deep-penetration welding, they might lead to insufficient welding seams. For example, welding of butt joints with small beam diameters require very high positioning accuracy and might therefore be not suitable. In addition, welding of an overlap configuration with small beam diameters may result in an insufficient connection width. An application example is the laser micro-welding of electrical connections of lithium-ion batteries. Here, the joint has to ensure a certain current flow and has to withstand mechanical forces. Therefore, a sufficient seam width has to be obtained [1].

To keep the advantage of high brilliance lasers, like high intensity to reach deep-penetration welding, but to ensure a sufficient seam width, the technique of spatial power modulation is applied. In this technique the weld feed is superposed with an oscillatory movement of high frequency. The superposed movement leads to a complicated pattern of the beam path, influencing quality and dimensions of the weld seam. Although, this technique has been introduced a couple of years ago it is still a topic of investigation [6, 8, 9].

In this work presented here, we investigate the irradiation pattern given by the spatial modulation, the seam dimensions and the temperature distributions for laser welding with this technique. To simplify the investigations, we make bead on plate welds and use a circular oscillatory movement, in contrast to linear oscillations [10, 11] or more complex Lissajous-type oscillations [12]. The welding experiments were made for contour welding with and without a superposed oscillatory movement of the laser beam. The oscillation amplitudes were varied, while laser power and welding velocity (feed rate) were kept at a constant ratio. The corresponding seam dimensions and cross-sections areas were investigated by micro cross-section cuts. To explain the seam pattern, we ran thermal simulations.

Spatial Power Modulation Technique and Principle of Spatial Power Modulation

In spatial power modulation (**SPM**) the feed rate is superimposed with a high frequent oscillating movement (Fig. 1). Due to the oscillation a perpendicular movement component is added in comparison to conventional welding, which results in an enlargement of the seam width. The general feed can either be generated by movement of the workpiece or deflection/movement of the laser beam.

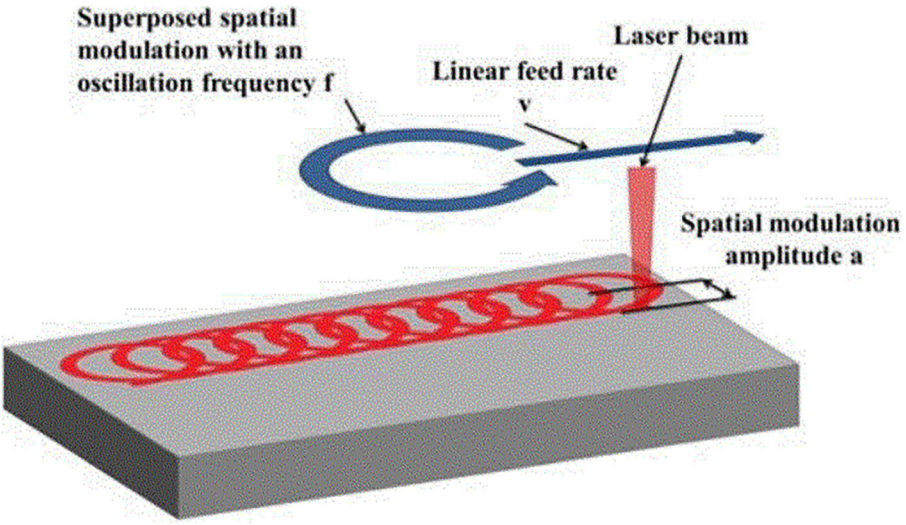

Fig. 1 Schematic of welding with spatial power modulation [2]

A high frequency movement and thus very fast beam movement can only be achieved by temporal varying deflection of the beam. The movement of the beam centre lies in a plane ((x, y)-plane) and is parameterized according to the equations shown in Table 1 (see also [6]).

As shown in Table 1 the velocity of conventional welding is the (constant) feed rate v_s, whereas in SPM welding the velocity has a sinusoidal component. The oscillatory movement can be implemented using scanner systems. Amplitudes and frequencies are then determined by the moveable mass of the mirrors in these systems. The basic setup of these systems is made by two rotatory mirrors in combination with a focussing lens (Fig. 2).

Advantages of scanner systems are high technical readiness, industrial distribution, system-integration possibilities and degrees of freedom in adapting the welding contour. The main disadvantage is the dependency of the amplitude on the oscillation frequency owing to the mass inertia of the mirrors and their motors. Other beam deflection systems allow the use of higher oscillation frequencies but lack the capability to transport high powers as they have high losses (e.g. acousto-optical deflectors) or low damage thresholds (e.g. MEMS). Therefore, the use of these systems for laser beam welding is limited to low power applications (e.g. welding of thin metal sheets) [13].

Table 1 Description of beam path with centre coordinates (x_c, y_c) and magnitude of the beam velocity or track speed v for conventional and SPM welding, v_s denotes the feed rate, f the oscillation frequency and a the oscillation amplitude (see Fig. 1)

path	$(x_c \;\; y_c) = (v_s t \;\; 0)$	$(x_c \;\; y_c) = (-\mathrm{a}\cos(2\pi ft) \;\; + v_s t \; \mathrm{a}\sin(2\pi ft))$
velocity	$v = \sqrt{\left(\frac{dx_c}{dt}\right)^2 + \left(\frac{dy_c}{dt}\right)^2} = v_s$	$v = \sqrt{(2\pi fa)^2 + v_s^2 + 4\pi f a v_s sin(2\pi ft)}$
	Conventional welding	Welding with SPM

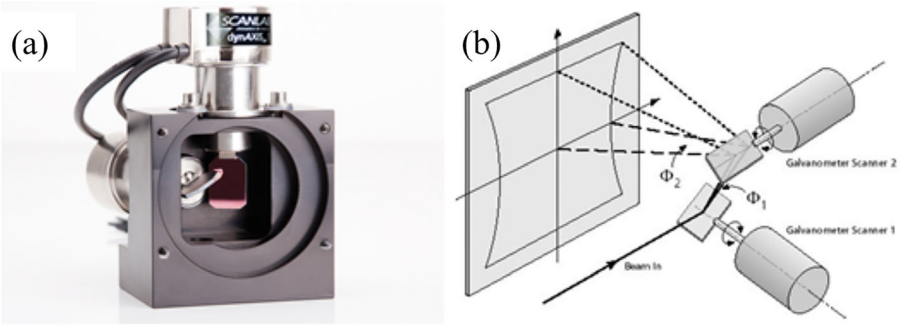

Fig. 2 **a** Deflection system from Scanlab, **b** principle for laser beam deflection systems with rotatory mirrors (Source: Scanlab GmbH)

Due to the oscillatory movement certain segments of the workpiece surface are irradiated multiple times, while others were not irradiated at all (Fig. 3). The segments and the number of irradiation events depend on the SPM parameters (amplitude, frequency, feed rate and beam diameter) and are calculated using the equation for the (x_c, y_c)-parameterisation above (Table 1).

Since the oscillatory and linear movements are superposed, not every part of the seam area in the (x, y)-plane is irradiated (Fig. 3). For example, along a central line ($y = 0$) some parts have not been irradiated, while along the edges ($|y| \cong a$) every part has been illuminated. Also, due to the direction of the feed rate, the irradiation pattern is not symmetric with respect to the central line. Furthermore, if the amplitude *a* is increased, the number of irradiation events along the edges also increases (cf. Fig. 3a and b). Increasing the feed rate v_s decreases the number of irradiation events (cf. Fig. 3b and c). A plane, positioned perpendicular to the feed rate and indicated by the black lines in Fig. 3, will be crossed by the laser beam at different y-positions. The y-positions and the number of crossings depend on the oscillatory parameters. The number of crossings increases with increasing amplitude but decreases with increasing feed rate (cf. Fig. 3). The crossing events might be seen indirectly in the micro cross-section cuts of the seam, if such an event is connected with localized melting and solidification. The newly formed crystal structure differs from the original structure of the base material.

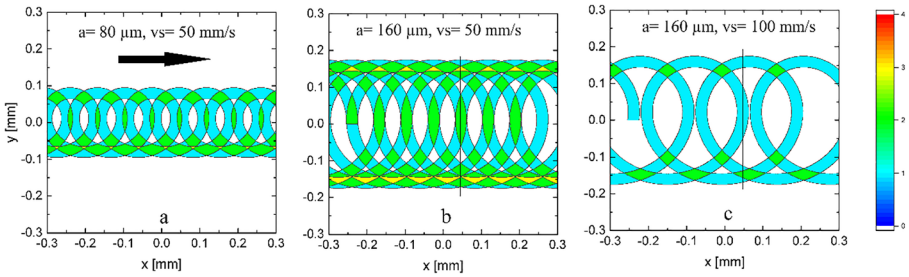

Fig. 3 Number of irradiation events for superposition of linear and circular-oscillatory movement of a laser beam for different amplitudes *a* and feed rates v_s, beam diameter:= 30 µm, frequency: = 700 Hz (rotation is counter clockwise), arrow indicate direction of feed rate, black lines see text

Table 2 Properties of experimental setup

Property of experimental setup	Numerical value
Central laser-emission wavelength (data sheet)	1070±10 nm
Focal length of focusing optics	163 mm
Focal diameter (measured)	~ 40 µm

Experimental Setup

The experiments were conducted as bead on plate welds with a SPI 400 W single-mode fibre laser and a 163 mm focusing optic. To characterize the optical parameters, a micro-spot monitor from Primes was used. The positioning of the specimen was ensured by a 3-axial-positioning table. For all experiments the focal position was placed on the workpiece surface. The specimens were $30 \times 100 \times 1.5$ mm^3 stainless steel (1.4301, AISI 304) samples.

A summary of the relevant laser parameters is given in Table 2.

Experimental Results

This section presents the results of the bead on plate welds. The dimensions of the seams are compared for contour welding without oscillatory movement and for SPM welding. The seam dimensions are visualized with micro cross-section cuts of the seam. The cuts were made perpendicular to the welding direction and represent the cross-section of the seam at a certain x-position. (see Fig. 4). Welds were produced at a laser power of 200 W, a feed rate of 50 mm/s and a frequency of 700 Hz, the shape of their corresponding seams were compared for different amplitudes. For zero amplitude and zero frequency, the process is equal to normal contour welding without oscillation. The shape of the seam has the typical "nail" -form, with a broad head at the upper part of the seam and a slender conical part below (Fig. 4, left). This "nail"-form is attributed to the flow dynamics of the melt near the surface. If a circular-oscillatory movement is superposed onto the linear feed rate, the depth of the seam decreases, while the width

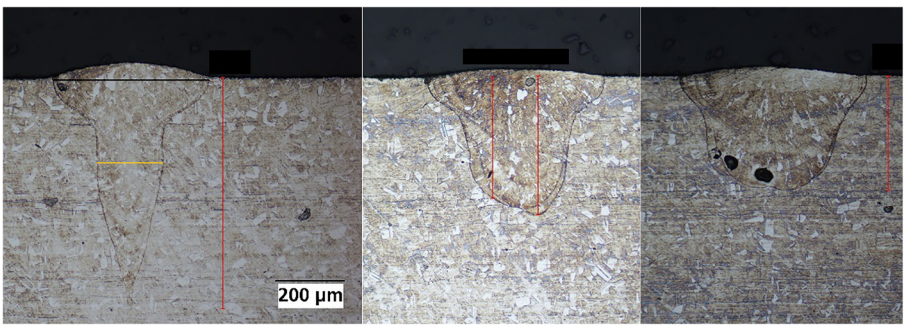

Fig. 4 Cross sections perpendicular to feed direction, $P = 200$ W, $d = 40$ µm, vs = 50 mm/s; left: $a = 0$, $f = 0$ Hz; middle: $a = 80$ µm, $f = 700$ Hz; right: $a = 160$ µm, $f = 700$ Hz (width *W0*: black line, width *W1/2*: yellow line, depth *D*: red lines)

Table 3 Seam width at the surface W0 and at half depth W1/2, seam depth D for different amplitudes a taken from Fig. 4, P = 200 W, vs = 50 mm/s, f = 700 Hz

Amplitude a/μm	$W0$/μm	$W1/2$/μm	D/μm
0	460	180	630
80	510	270	400
160	530	370	330

increases, the "nail"-form becomes less pronounced with increasing amplitude. Furthermore, at the lower part of the seam, successive melting and freezing (solidification) zones can be observed. They are associated to the moving laser beam, which crosses the plane of the cross section several times at different positions as discussed in Section 2. Although the number of crossings increases with increasing amplitude, the number of visible solidification zones does not (cf. Figure 4, middle and right). This might be explained by examining the positions of the crossings. At an amplitude of 160 μm, they are bunched near the edges, and not all solidification boundaries can be distinguished. Furthermore, if the crossing plane stays in a molten state between two crossing events, the events cannot be distinguished.

The seam widths are measured at two positions: at the surface (*W0*) and at half depth of the seam (*W1/2*) (see Fig. 4). The results are summarized in Table 3. Due to the oscillatory movement of the beam, the lower limit of the width is about two times the amplitude. Heat conduction and melt flow make it broader.

Increasing the amplitude from 0 to 160 μm also increases the width *W0*, but not to the same proportion (Table 3). For contour welding without oscillatory movement the widths *W0* and *W1/2* are determined by heat conduction and melt flow near the surface [14, 15]. For oscillatory movement the width is also determined by the amplitude. Particularly for the width at mid-position W1/2 the lower limit of the width is approximately the twofold of the amplitude. The depth D of the seam decreases with increasing amplitude (see Tables 3 and 4).

In the following welding experiments the laser power was increased to 400 W and the feed rate to 100 mm/s.

Although, the energy input per section E_S (= P/vs) in these experiments is the same as in the previous case, the depth is considerable larger (Table 4).

For seams generated by the oscillatory movement the different solidification zones can be seen, especially in the lower part of the seam. There are also zones that have not been molten during the welding process, giving the seam a spiky appearance in the lower part (Fig. 5, right). So, the shapes of the cross section differ for both feed rates

Table 4 Seam width at the surface *W0* and at half seam depth *W1/2*, seam depth *D* for different amplitudes *a* taken from Fig. 5, *P* = 400 W, vs = 100 mm/s, *f* = 700 Hz, **D* equals the thickness of the sample

Amplitude a/μm	$W0$/μm	$W1/2$/μm	D/μm
0	340	150	1000*
80	410	210	930
160	510	340	720

and amplitudes. This may be attributed to the different irradiation pattern shown in Fig. 3, and the corresponding temporal development of the molten volume. Therefore, we introduce a simplified thermal model in section 5 to discuss the influence of the modulated heat input on the dimensions of the molten volume for both feed rates.

Tables 3 and 4 show that the depth of the seam obtained for 400 W laser power is approximately twice the one obtained for 200 W. The difference of the seam widths W0 and W1/2 are less pronounced.

This is attributed to the heat input and the heat loss of the process. To discuss the dependence of heat input and heat loss on the seam dimensions, the area of the seam cross-sections (A) are measured and compared. The measurements are taken from micro cross-section cuts (e.g. Figs. 4 and 5) for different amplitudes (not all cuts are shown). The amplitudes are varied between 80 and 300 µm. Larger amplitudes cannot be obtained for 700 Hz, because of the inertia of the rotatory mirrors (cf. Section 2).

As shown in Fig. 6, for constant E_s area A increases along with feed rate and laser power, because the penetration depth increases significantly, while the width doesn't change much (cf. Tables 3 and 4). To explain this fact, it is noted that with increasing feed rate the heat loss from the laser-material interaction zone into the surrounding material decreases. Thus, for deep-penetration welding with constant E_s the penetration depth increases, and the seam width decreases with increasing feed rate. If the feed rate is increased at constant laser power, E_s and the depth decreases. But due to the reduced heat loss, the decrease is not proportional to the inverse of the feed rate ($1/v_s$) [5, 16]. This leads to a weak dependence of the depth on the feed rate or beam velocity.

Furthermore, area A increases with increasing amplitude until a local maximum is obtained. For 200 W the amplitude of the maximum is 220 µm. For 400 W the maximum amplitude lies outside the experimental range, but for amplitudes above 160 µm area A is nearly constant (Fig. 6).

The existence of a local maximum is explained by two effects. First, with increasing amplitude the width of the seam increases (Tables 3 and 4). Therefore, the track speed

Fig. 5 Cross sections perpendicular to feed direction, $P = 400$ W, $d = 40$ µm, vs = 100 mm/s; left: $a = 0$, $f = 0$ Hz; middle: $a = 80$ µm, $f = 700$ Hz; right: $a = 160$ µm, $f = 700$ Hz (width *W0*: black line, width *W1/2*: yellow line, depth *D*: red lines)

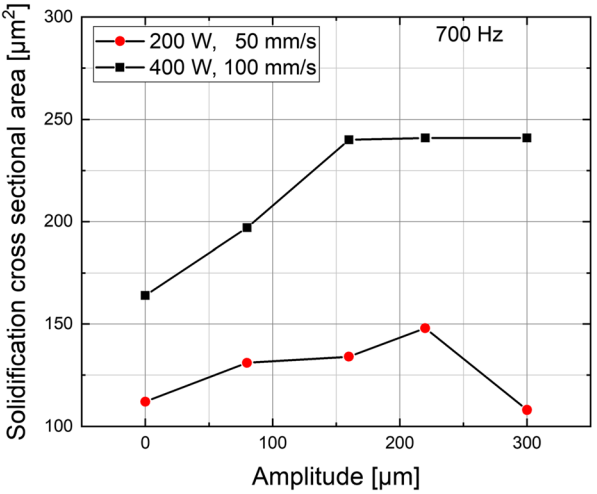

Fig. 6 Solidification cross sectional area vs. oscillation amplitude

increases approximately in the same way (see Table 1). This leads to a reduction of keyhole and seam depth. But, as state above, the keyhole depth has only a weak dependence on the track speed and, thus, on the amplitude. Therefore, area A increases with the amplitude. Second, increasing the amplitude above the maximum value, the track speed becomes too high to create enough keyhole depth. And, along with a decreasing aspect ratio, the deep-penetration effect decreases, meaning that less laser power will be delivered to the work piece. Thus, a shift towards the heat conduction welding regime can occur. Both result in a lower weld depth and smaller area *A*.

Thermal Simulation Results

This section outlines a simplified thermal model of the deep-penetration welding process and discusses the results. The aim is to investigate the development of the molten volume. The molten volume is the area of the workpiece where the temperature exceeds the melting temperature. Beside the heat input, the temperature is determined by the heat conduction of the material. In the molten volume also a melt flow occurs, which gives a convective heat flow. This results in the typical nail form of the seams (see Figs. 4 and 5).

As mentioned in section 4, the influence of the melt flow on the seam dimensions decrease with increasing oscillation amplitude. Furthermore, with increasing distance from the surface the influence of the flow field on the seam dimensions decreases. Thus, the flow field is neglected for the thermal simulations, and the temperature is obtained by the heat conduction equation

$$\rho c_p \frac{\partial T}{\partial t} + \nabla(K \nabla T) = Q(P, w_0, d_k, v_s, f, a),$$

where ρ, c_p and *K* are mass density, specific capacity and heat conductivity, respectively. They are functions of the temperature and are taken from [17].

The heat source Q depends on laser power P, beam/keyhole diameter w_0, keyhole depth d_k, feed rate v_s, oscillation frequency f and amplitude a. In this ansatz Q is represented as a volumetric heat source, ignoring the detailed dynamics of the keyhole surface, as well as vapor or plasma formation. To justify this approach, the keyhole volume and the volume of the molten material are compared. The keyhole volume is much smaller than the molten volume because it scales with the beam diameter w_0, while the molten volume scales with the width W1/2. Thus, the influence of the actual keyhole model on the dimensions of the molten volume will be small.

As discussed above for deep penetration welding a large part of the laser beam is absorbed inside the keyhole. For the simulations it is assumed that 100% of the laser power is delivered to the workpiece. Furthermore, the diameter of the keyhole w_0 is taken as a constant throughout the entire keyhole depth d_K, which is set to the measured depth D presented in Tables 3 and 4. The volumetric heat source is given according to following equation

$$Q = \frac{4\,P}{\pi w_0^2 d_k} F(x, y, z; d_K, w_0, a, f)$$

where the function F represents the spatial and temporal distribution of the heat source. The function F is applied in the following form

$$F = exp\left[-\left(\frac{2|\boldsymbol{r}-\boldsymbol{r}_c(t)|}{w_0}\right)^n\right]\theta(d_K + z)$$

The vector $\boldsymbol{r}_c$ is the position of the beam centre (see Table 1), depending on the oscillation amplitude, the frequency and the feed rate; θ is the Heaviside function and n a Super-Gaussian factor. For the simulations $n = 8$ is taken to make the slope of the exponential function sufficiently steep.

The thermal simulations are carried out with the FEM-software Comsol Multiphysics®. The initial temperature of the model workpiece is 20 °C and the heat source moves according to the movement of the laser beam, with a feed rate in x-direction (cf. Fig. 1). The model workpiece and the mesh structure are shown in Fig. 7. To save computation time the model geometry is divided in two parts. An inner part with a fine and an outer part with a coarse meshing. The inner part is the region where the moving laser beam interacts with the material. The outer part ensures the heat flow from the interaction area.

The molten volume is represented by an isotherm surface with the melting temperature of steel (1.4301, AISI 304), which is set to 1450 °C. To distinguish between the different features of the isotherm surfaces for 200 and 400 W, the z- and x-projections of the surfaces are shown as snap shots in Figs. 8 and 9.

The snap shots were taken at the moments were the position of the laser beam is near its turning point along the feed- or x-direction at $y \approx 0$.

As seen in Fig. 8 the dimensions of the molten volume differ as the feed rate changes. At 50 mm/s the heat diffuses fast enough to keep pace with the laser beam, resulting in a compact form of the isotherm surface. For 100 mm/s the ahead running laser beam produces a distinctive molten zone, which is separated from the bulk zone (Fig. 8, right). This can be explained with the irradiation pattern shown in Fig. 3 and

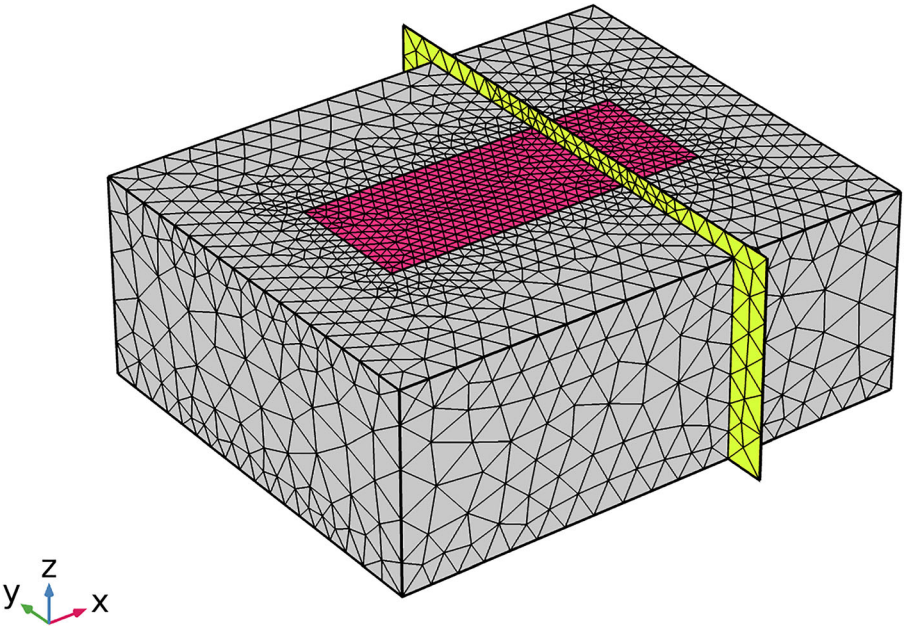

Fig. 7 Model geometry of the work piece and mesh structure, inlay with a finer mesh to ensure spatial resolution of the moving laser beam, outer part with a coarse mesh, yellow plane is perpendicular to weld direction (see text)

also with the path of the beam shown in Fig. 8. For a feed rate of 50 mm/s the irradiation pattern has a higher density than for 100 mm/s. Especially, the distance between the irradiation events along the centre axis (y = 0) increases with increasing feed rate. For 100 mm/s the distance is large enough to create distinctive molten zone, which is separated from a bulk zone. For 50 mm/s the distance is too small, and the heat conduction can bridge it.

The x-projection along the feed rate is the time dependent equivalent of the cross sections shown in Figs. 4 and 5.

The simulations for 100 mm/s show that the distinctive molten zone, which runs ahead of the bulk zone, reaches deeper into the material than the following bulk zone

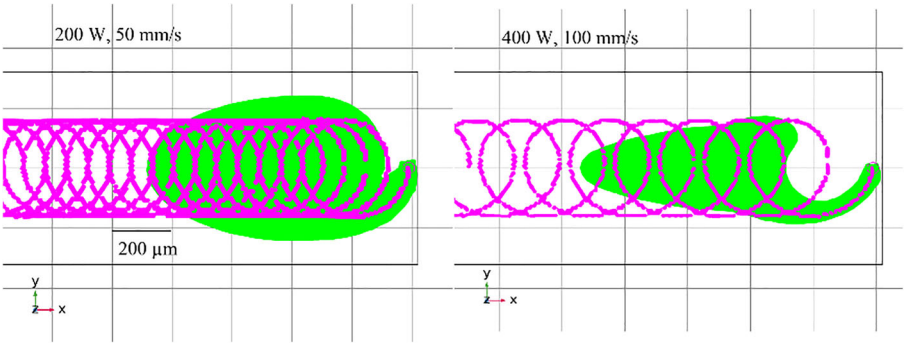

Fig. 8 Snap shot of the z-projection of the 1450 °C-isotherm surface (green) of the simulated welding process with an amplitude of 160 µm and the path of the laser beam (magenta, line width is **not** beam width, rough appearance due to numerical inaccuracies), left: $P = 200$ W, vs = 50 mm/s, right: 400 W, 100 mm/s

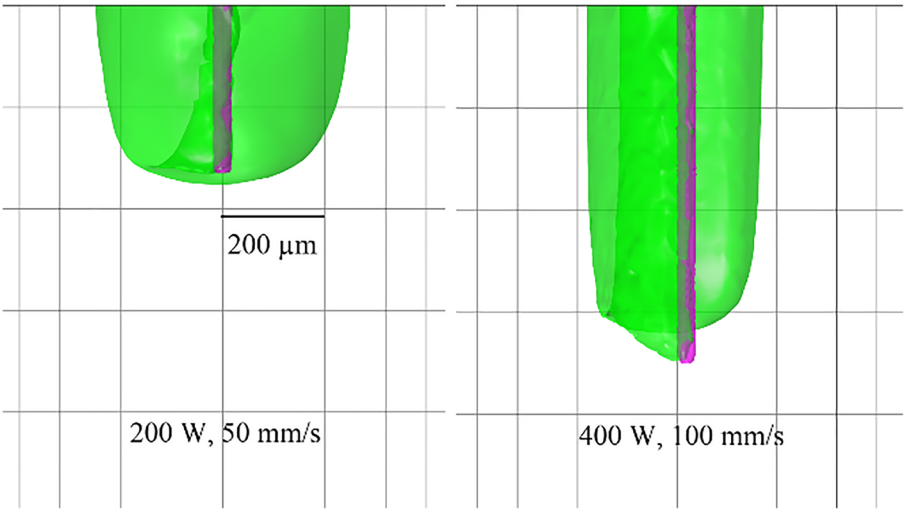

Fig. 9 Snap shot of the x-projection of the 1450 °C-isotherm surface (green) of the simulated welding process with an amplitude of 160 µm and actual position of the model-keyhole (magenta), left: $P = 200$ W and vs = 50 mm/s, right: 400 W and 100 mm/s, surfaces with artificial lighting to show the 3D-structure of the molten volume, isotherm surfaces are semi-transparent

(Fig. 9, right). For 50 mm/s this separation is not visible, and the bulk zone defines the dimensions of the seam (Fig. 9, left). For 100 mm/s, beside the bulk zone, the ahead running distinctive zone defines the appearance of the lower part of the seam. This correlates with the cross sections of Figs. 4 and 5 for an amplitude of 160 µm. From this one can conclude that the seam dimensions will change along the weld direction for high feed rates. The dimensions of the cross-section cuts, especially at the lower part of the seam, will differ, depending on the position.

This can be visualized by monitoring the temperature on a plane, which is shown in Fig. 7. Hence, a function A_m is defined with the following property: if the temperature at a point (x, y, z) stays below the melting temperature T_m during the entire processing time, the value of A_m at that point is zero, otherwise it is one. The corresponding equation is as follows

$$A_m(x,y,z) = \left\{ \begin{array}{l} 0, T(x,y,z,t) < T_m \\ 1, T(x,y,z,t) > T_m \end{array} \right\}.$$

If the values of function A_m are presented at different x-positions x_i, $A_m(x_i, y, z)$ resembles the cross-sections of the model seam. The results for three positions each 50 µm apart are shown in Fig. 10.

On the one hand, for the smaller feed rate (Fig. 10, upper row), the seam dimensions are given by the bulk part of the molten volume and, therefore, the shape remains approximately the same at all position. On the other hand, for the larger feed rate the shape differs at different positions. In the lower part the shape of function A_m appears with two side peaks, two side peaks and a center hump and a plateau shape at the three different x-position (Fig. 10, lower row, from left to right). In the upper part the shape of function A_m remains the same.

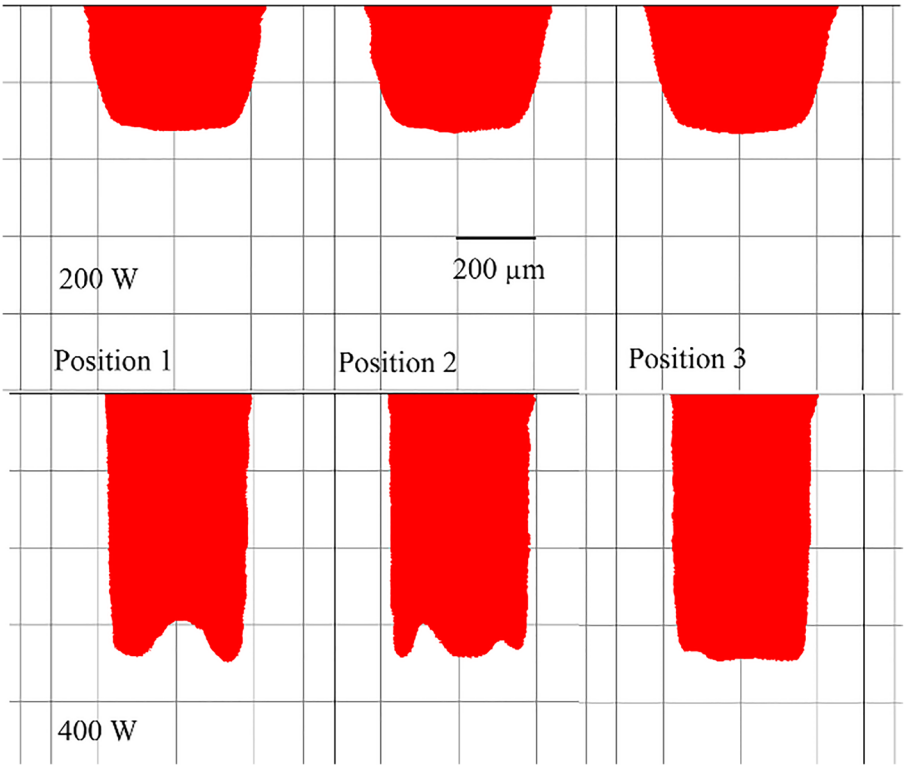

Fig. 10 Function A_m calculated for three x-positions, top row: P = 200 W, v_s = 50 mm/s, bottom row: P = 400 W, v_s = 100 mm/s, function A_m gives the position where the temperature had exceeded the melting temperature, distance between positions is 50 µm

The dimensions of function A_m - the cross-section of the model seam - only roughly match with the cross-sections of Figs. 4 and 5 because the model neglects the flow and keyhole dynamics. But the model provides an insight how the heat input, according to the irradiation pattern of Fig. 3, influences the development of the molten volume, and the appearance of the welding seam.

Conclusion

The paper presents an examination of seam formation in laser beam micro-welding with spatial power modulation. The seam formation has been analyzed using micro cross-section cuts of the seams, and the solidification cross-section area has been evaluated. Thermal simulations show that temporal behavior of the molten volume depends on the irradiation pattern and the heat conductivity, giving rise to different solidification structures of the seam. When spatial power modulation is used, the seam width and depth can be adapted in a certain range without any changes to the optical setup. In general, spatial power modulation decreases the weld depth, but increases the seam width in such a way that the cross-section area of the seam increases as amplitude increases until a local maximum is obtained. The position of the maximum depends on the power; higher power results in a larger maximum amplitude.

Funding Open Access funding enabled and organized by Projekt DEAL.

References

1. Heinen, P., Haeusler, A., Mehlmann, B., Olowinskiy, A.: Laser beam microwelding of Lithium-ion battery cells with copper connectors for electrical connections in energy storage devices. Lasers Eng. **36**, 147–167 (2017)
2. Mehlmann, B., Gehlen, E., Olowinsky, A., Gillner, A.: Laser micro welding for ribbon bonding. Phys. Procedia. **56**, 776–781 (2014)
3. Locke, E., Hoag, E., Hella, R.: Deep penetration welding with high power CO2 lasers. Weld. Res. Suppl. **51**, 245–249 (1972)
4. Miyamoto, I., Maruo, H.: Evaporation characteristics in laser welding - fundamental study on theoretical modelling of laser welding (Report 2). Weld. Int. **10**(6), 448–453 (1996)
5. Engler, S., Ramsayer, R., Poprawe, R.: Process studies on laser welding of copper with brilliant green and infrared lasers. Phys. Procedia. **12**, 339–346 (2011)
6. Schmitt, F., Mehlmann, B., Gedicke, J., Olowinskiy, A., Gillner, A., Poprawe, R.: Laser beam micro welding with high brilliant Fiber lasers. JLMN. **5**(3), 197–203 (2010)
7. Beyer, E., Bakowsky, L., Loosen, P., Poprawe, R., Herziger, G.: Development and optical absorption properties of a laser induced plasma during CO2-laser processing, In: D. Schuoecker (Ed.), Industrial Applications of High Power Lasers. SPIE, pp. 75–80 (1984)
8. Hollatz, S., Ryan, C., Olowinsky, A., Gillner, A., Poprawe, R.: Measurement of Keyhole Depth during Laser Beam Micro Welding with Scanners, Proceedings of LPM2018, pp. 1–5 (2018)
9. Heinen, P., Eichler, F., Haeusler, A., Aden, M., Gillner, A., Poprawe, R.: Influence of spatial power modulation on pore and crack formation in laser beam welding of aluminum. J. Laser Appl. **31**(2), 022013 (2019)
10. Kraetzsch, M., Standfuss, J., Klotzbach, A., Kaspar, J., Brenner, B., Beyer, E.: Laser beam welding with high-frequency beam oscillation: welding of dissimilar materials with brilliant Fiber lasers. Phys. Procedia. **12**, 142–149 (2011)
11. Rubben, K., Mohrbacher, H., Leirman, E.: Advantages of using an oscillating laser beam for the production of tailored blanks. Proc. SPIE. **3097**, 228–241 (1997)
12. Thiel, C., Hess, A., Weber, R., Graf, T.: Stabilization of laser welding processes by means of beam oscillation. Proc. of SPIE 84330V-1-10 (2012)
13. Schmitt, F.: Laserstrahl-Mikroschweißen mit Strahlquellen hoher Brillanz und örtlicher Leistungsmodulation, Berichte aus der Lasertechnik. Shaker, Aachen (2012)
14. Beck, M., Berger, P., Dausinger, F., Hügel, H.H.: Aspects of keyhole/melt interaction in high speed laser welding. Proc. SPIE. **1397**, 769–774 (1990)
15. Klemens, P.G.: Heat balance and flow conditions for electron beam and laser welding. J. Appl. Phys. **47**(5), 2165–2174 (1976)
16. Shimokusu, Y., Fukumoto, S., Nayama, M., Ishide, T., Tsubota, H.: Application of high power YAG laser welding to stainless steel tanks, Mithsubishi heavy industries ltd. www.mhi.co.jp/technology/review/pdf/e381/e381001.pdf. pp. 118–121 (2000)
17. Kim, C.S.: Thermophysical Properties of Stainless Steels. (1975). https://inis.iaea.org/search/search.aspx?orig_q=RN:7236394